



Article

Deciphering Complex Morphology and Structural Connectivity of High-Magnitude Deep-Seated Landslides via Airborne Laser Scanning: A Case Study in the Vrancea Seismic Region, Romanian Carpathians

Mihai Micu ¹, Mirela Vasile ^{2,*}, Florin Miron ^{3,4}, Alexandru Onaca ⁵ , Flavius Sîrbu ^{5,6}
and Skyline Drones Team ⁷

¹ Institute of Geography, Romanian Academy, Dimitrie Racovita 12, Sector 2, 023993 Bucharest, Romania; mikkutu@yahoo.com

² Division of Life, Earth and Environmental Science, Research Institute of the University of Bucharest, Panduri 90, 050663 Bucharest, Romania

³ Faculty of Geography, University of Bucharest, Nicolae Bălcescu 1, 010041 Bucharest, Romania; florin.miron@s.unibuc.ro

⁴ TERRASIGNA Logofat Luca Stroici 3, 020581 Bucharest, Romania

⁵ Department of Geography, West University of Timișoara, V. Pârvan 4, 300223 Timișoara, Romania; alexandru.onaca@e-uvv.ro (A.O.); flavius.sirbu@e-uvv.ro (F.S.)

⁶ Institute for Advanced Environmental Studies, West University of Timișoara, Oituz 4, 300086 Timișoara, Romania

⁷ Skyline Drones Romania, Anton Pann 1, 300102 Timișoara, Romania; office@skylinedrones.ro

* Correspondence: mirela.vasile@geo.unibuc.ro



Citation: Micu, M.; Vasile, M.; Miron, F.; Onaca, A.; Sîrbu, F.; Skyline Drones Team. Deciphering Complex Morphology and Structural Connectivity of High-Magnitude Deep-Seated Landslides via Airborne Laser Scanning: A Case Study in the Vrancea Seismic Region, Romanian Carpathians. *Remote Sens.* **2023**, *15*, 5286. <https://doi.org/10.3390/rs15225286>

Academic Editors: Enrico Corrado Borgogno Mondino, Daniele Giordan, Lisa Borgatti, Stefano Gandolfi and Alessandro Corsini

Received: 25 August 2023

Revised: 18 October 2023

Accepted: 19 October 2023

Published: 8 November 2023



Copyright: © 2023 by the authors. Licensee MDPI, Basel, Switzerland. This article is an open access article distributed under the terms and conditions of the Creative Commons Attribution (CC BY) license (<https://creativecommons.org/licenses/by/4.0/>).

Abstract: In the Vrancea seismic region (Romanian Carpathians; the most important intermediate-depth seismic source of Europe), the morphology of the slopes is often marked by the existence of numerous high-magnitude, deep-seated active, dormant or relict landslides, which are the subjects of many cases of functional and structural connectivity. Due to the compact and extensive (coniferous and broad leaved) forest coverage and because of the lack of publicly available regional high-resolution DEMs, it is usually difficult to fully understand the morphogenetic framework of such large, deep-seated landslides in order to assess their frequency–magnitude relationship, a key issue in hazard quantification. However, the high impact of such landslides on river networks requires an in-depth understanding of the multi-hazard framework, as cascading effects are likely to affect the presently growing human activities developing along the valleys. Within a case study represented by a 2.5 km long deep-seated landslide, that caused a 500 m lateral occlusion of Buzău River, we used integrated remote sensing technologies (UAV laser scanning) and in situ (geomorphic mapping and ERT investigations) techniques, which allowed us to better understand the structural connectivity which conditions the landslide hazard in such complex morphogenetic conditions, outlining the present potential of the regional seismo-climatic context to trigger potential high-magnitude chain effects.

Keywords: structural connectivity; LiDAR; deep-seated landslides; Vrancea seismic region

1. Introduction

Landslides represent some of the most complex geomorphic processes, responsible for slope and channel modeling under various conditioning, preparing and triggering factors. Besides the fundamental implications of landslide studies in terms of the assessment of agents, processes or forms that allow the in-depth understanding of slope and river system interactions through depletion, erosion, transport and accumulation, their applied importance is even greater. It has been outlined that, during the last decades,

strong evidence of faster exposure of assets and individuals to landslide risk has been reported, in comparison with the decrease in vulnerability [1]. Despite the overall important advancement in landslide hazard research, this exposure–vulnerability connection may be perceived mainly within local communities; they frequently lack proactive measures (resulting from livelihood conditions, settlement locations, social bonding and educational availability for prevention/preparedness activities), thus not allowing them to enhance the risk perception in order to reduce the level of potential consequences. Large, deep-seated landslides prove to be especially difficult to evaluate in terms of trigger (usually, more than just a single one) and frequency–magnitude relationship, frequently being subject to environmental preparing and triggering factors different from those of present times. Subsequently, their relict or dormant characters are not promoting them as key elements in susceptibility evaluation [2], while their reactivation potential is not always taken into consideration; meanwhile, through their (very) low frequencies, large, deep-seated landslides may even disappear from the collective mind as serious, threat-posing mass movements, allowing the present development of economic activities in areas prone to local (to even total) reactivations.

Due to their rather local behavior, the role and place of mass movement (including landslides) processes was largely substituted and reduced to punctual manifestations of (extremely) short intensity within early theories regarding the evolution and modeling of landforms [3–5], and only during the last decades was it outlined that such processes can impose themselves by imprinting specific patterns of slope evolution in numerous mountain and hilly regions [6–11]. In this framework, in 1971, Chorley and Kennedy [12] adapted the complex system theory to geomorphology, promoting the morphological, cascading, process–response and control systems, outlining the transfer of energy and matter within the system and between landforms through the concept of connectivity, which has been widely used since then. Equally studied by ecologists and hydrologists (as described by review studies such as [13–15]), the connectivity (sediments, landscape and hydrological), following a general geomorphic approach, describes and quantifies the linkages between sediment source areas and the corresponding sinks in catchment systems.

Connectivity assessment (and especially quantification) from local to regional scales is still marked by consistent uncertainties derived from the complex geomorphic patterns and processes of slope and channel systems [13,16]. This applies to two connectivity categories: functional (through stream-level interactions; the processes associated with the sources and fluxes of water and sediments within contiguous/isolated system components) and structural (through physical connections, depending on the position and more-or-less distant spacing of interfering landscape units) [17–22]. As described in the literature above, analyzed within a 117-paper review by Najafi et al. [21], structural connectivity is commonly regarded as a physical concept that denotes the physical linkage of various landscape components, with a focus on static characteristics (like landform topography and morphology or vegetation pattern) at different spatiotemporal scales. In comparison, functional sediment connectivity is generally regarded as a process-based concept derived from system process dynamics. In this framework, the understanding of structural connectivity as highlighted by representative case studies generally enables and improves the comprehension of the nonlinear response of the slope–channel coupled with external forcing, allowing the quantification of the direct and indirect impacts during following research phases. Additionally, it influences the thresholds of magnitude and duration necessary to create fluxes between individual landscape units [23,24]. In this context, in this paper, we will focus on structural connectivity in terms of physical adjacency, spatial configuration of potential sediment sources and accessibility and their potential movement along the slope, opening the perspective of detailed functional sediment connectivity evaluation and quantification, focusing on sediment detachment and sediment transport and deposition processes.

In particular, the typological, the morphodynamic and morphologic complexity of landslides in geomorphically active regions (like the Vrancea seismic region) are enhancing

the challenges in susceptibility and hazard evaluation, as key steps in analyzing, evaluating and managing the risk. Moreover, in such seismically active regions, the potential conditioning or overlapping of climatic and seismic triggers are also enhancing the multi-hazard context, especially in the case of high-magnitude landslides, whose morphology might raise problems in fully understanding the occurrence mechanisms and the (paleo)environmental conditions during the initiation time. Their impact on the slope–channel systems interface is major, and may result in consistent lateral and longitudinal morphometric changes, not only important from a fundamental point of view (river course change, temporary or permanent valley blockage) but also from an applied one.

We focus our analysis on such a case study of a large and complex landslide with unknown morphodynamics and a complex and unclear morphology, impacting the most important transcarpathian river valley of the entire area in a major way. Its clearly superior size, compared to any present-day existing mudflow or debris flow in the region, is also an element that must be taken into account, thus raising an intriguing question: what specifically triggered a process of such a magnitude (it is out of the ordinary, so it remained either uncharted or, at best, just partially mapped), with a presumed sudden character of displacement and accumulation, in the condition of a slope that is neither very long nor extremely inclined? These questions are raising awareness for the necessity of a complete understanding of this case study; of its complex morphogenesis and structural connectivity patterns of a (rather uncommon) high-magnitude and vegetated deep-seated landslide. For this purpose, it is the intent of this paper to (1) perform an accurate, remote sensing (UAV)-supported geomorphological mapping of the landslide in order to (2) analyze the high-impact structural connectivity in terms of the physical linkage of various landform components which will allow us to (3) evaluate the frequency of high-magnitude landslides that can be locally and regionally responsible for cascading effects.

2. Study Area

The general study area corresponds to the contact between the (SE) Curvature Carpathians (low- and medium-altitude mountains, developed below 1800 m and locally built on Paleogene flysch formations of less cohesive and compact sandstones, forming thinner or thicker packages, alternating with thicker schistose intercalations of clays and marls) and the Curvature Subcarpathians (association of 400–900 m high hills and lower depressions built on less-hard Mio-Pliocene molasse deposits—sandstones, sands, clays, marls, tuff, salt breccia and gypsum—accumulated in the Carpathian foredeep). The river valleys, the environments most subjected to these processes, are densely inhabited and experiencing an increase in human activities (tourism), leading to higher values of exposure and vulnerability [25]. In the Vrancea seismic region, the propitious conditioning/preparing/triggering framework is leading to a wide spectrum of landslides [26,27], as outlined in Figure 1.

In general terms, there are recent detailed descriptions of this landslide-prone environment resulting from the analysis of their preconditioning, preparing and triggering factors, and focusing on the landslides' morphogenetic complexity, types and spatial patterns [27,28], land-surface variables for landslide detection [29], DEMs and sampling design for landslide susceptibility modeling [30–32], climatic and seismic triggering factors [33–35] and exposure assessment [36].

Large, deep-seated landslides, many of them considered dormant and relict [37], have not been intensively studied yet, for several potential reasons, for example, the lack of detailed cartographic materials to help with understanding the morphology/morphometry, the lack of absolute age dating and the lack of accurate, very high resolution (multi-temporal) DEMs. Meanwhile, slope and channel morphologies have many times witnessed the impact of such large, deep-seated landslides, which due to the high magnitude, age and vegetation cover, remained uncharted in the absence of a good, high-accuracy DEM. This is the case of the Pältineni landslide, a large, deep-seated landslide which caused the deflection of the Buzău River 450–500 m westwards. Possibly because of its much larger

size in comparison with any landslides that occurred during the last century, the Pältineni landslide has only been mentioned a few times as an important slope process, as its contour began to form a better shape once accurate (color) aerial images started to become publicly available during the first decade of the XXI century [38,39].

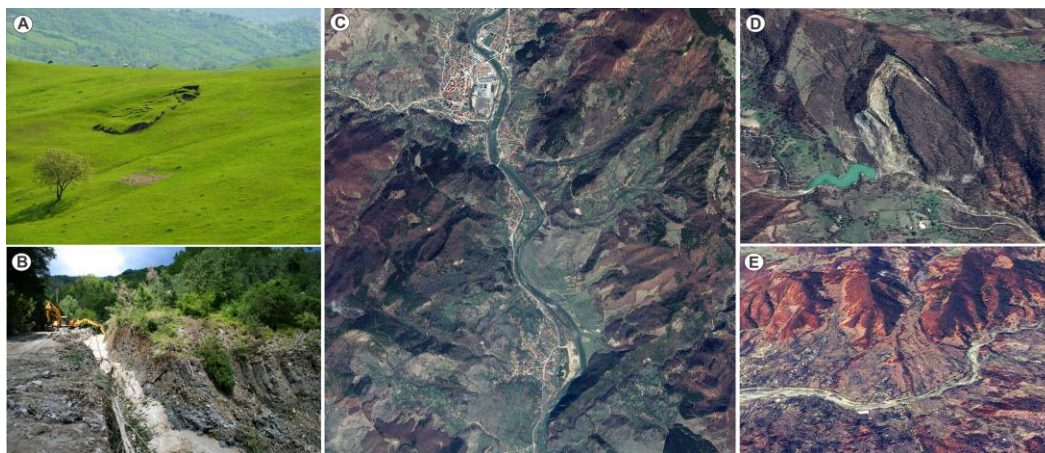


Figure 1. Examples of geomorphologic impact and impact surface characteristics of structural connectivity in Vrancea seismic region, reported for the classification of Korup [40]: (A) buffered, null superior; (B) riparian, punctual-linear; (C) occlusion, areal; (D) blockage, areal; (E) obliteration, areal. Image sources: (A,B): photos by Mihai Micu; (C–E): aerial images provided by Google Earth archive.

The Pältineni landslide is situated in the Buzău sector of the Curvature Carpathians (Figure 2). Located on the left slope of the Buzău River, downstream from the confluence with the Nehoiu stream, the Pältineni landslide (debris flow) extends over a length of 2.5 km, between 800 and 350 m a.s.l. Its main source areas (both old and recent, as it will be later detailed) cover a total of 80 ha, its runout channel covers 6 ha and its accumulation terminal fan covers 35 ha. The flow-like process (a characteristic outlined by its morphology, which clearly depicts the three typical morphodynamic sectors of depletion, runout and accumulation) shows several stages of reactivation, the most recent ones (presently active) situated in the lower part of the toe.

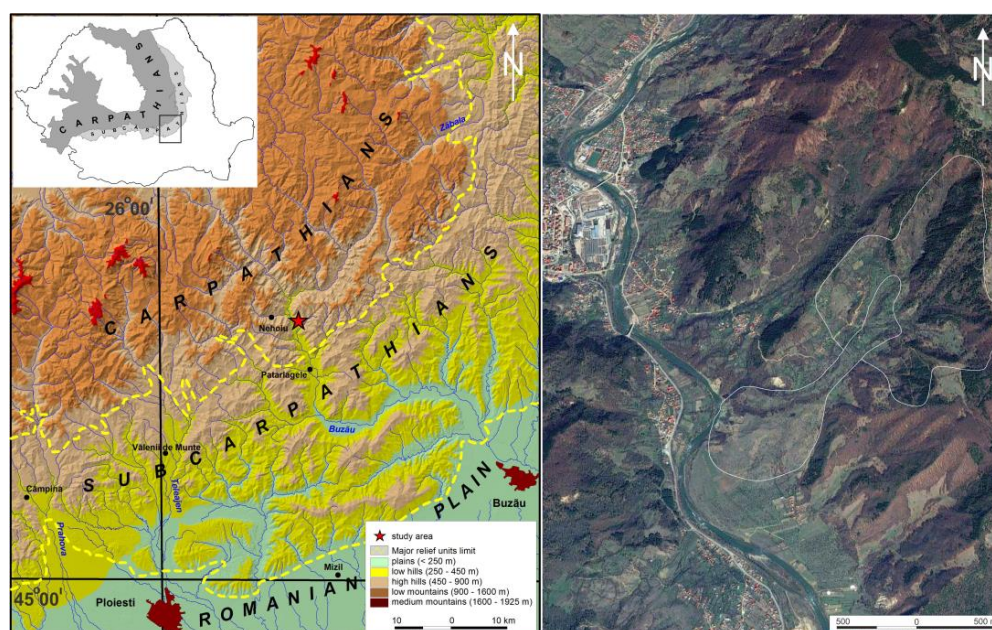


Figure 2. The location of the study area in the Buzău Carpathians, Vrancea seismic region. Aerial image source: Google Earth image archive.

Its terminal sector of accumulation is the most clearly outlined in slope morphology and is arranged in the form of a fan extended on about 35 ha, massive and compact, without reflecting different sequences or multiple phases of accumulation in its morphology (which is similar, for example, to the presently active Chirlești earth flow, located 3.5 km downstream; ref [41]). With a thickness of up to 40–50 m, the (estimated) volume of the cone, about 5 million m³, caused an obliteration of the Buzău River and its sudden deviation some 450–500 m westwards. The arguments for a sudden movement are emerging from several morphological and morphometrical considerations: (i) The compact profile of the cone (in comparison with the small-size current reactivations caused by the lateral erosion of the Buzău River, which is evident in its northeastern extremity), of a relatively younger age (compared to the similar process which occurred immediately to the north, where the former village of Bădârlegiu—currently a neighborhood of the city of Nehoiu—developed on a cone that is similar, but older and presently completely and straightly cut by the Buzău River); (ii) the change in the river direction towards the exit from the Păltineni basin back on a course that can be connected to the upstream one; and (iii) the arrangement of the compact mass of debris over old terrace formations (described in the following).

Despite the high magnitude of the landslide (at least two to four times the length and surface/volume of the main source area or the accumulation fan with respect to Chirlești, Valea Viei, Rotarea or Târlești, to list the most representative ones; see Figure 3 for comparison) and its obvious impact on the Buzău River, its contour was never represented with accuracy. The most visible sector (the accumulation fan) appears most clearly represented on medium-scale geological maps (Figure 4C,D), while on geomorphic maps, sketches or aerial photo interpretations, it appears either as not existent (Figure 5C), partly mapped and with an uncertain location (Figure 5A,D,E) or as a misleading interpretation (as a shallow landslide; Figure 5B).

There could be several explanations for this: the very large magnitude of the landslide (exceeding any similar, present-day processes); the dense vegetation cover, not allowing a clear delimitation of the morphodynamic sectors; the lack of high-accuracy aerial photos (the first modern ones, in color, only date from 2004 to 2008); or the lack of an accurate (LiDAR) regional DEM (the first one, inaccessible to the public, without a regional continuity and covering only the immediate vicinity of flood plains, was produced for this part of the Carpathians during the 2010–2014 period, during the implementation of the EC 2007/60 Flood Directive).

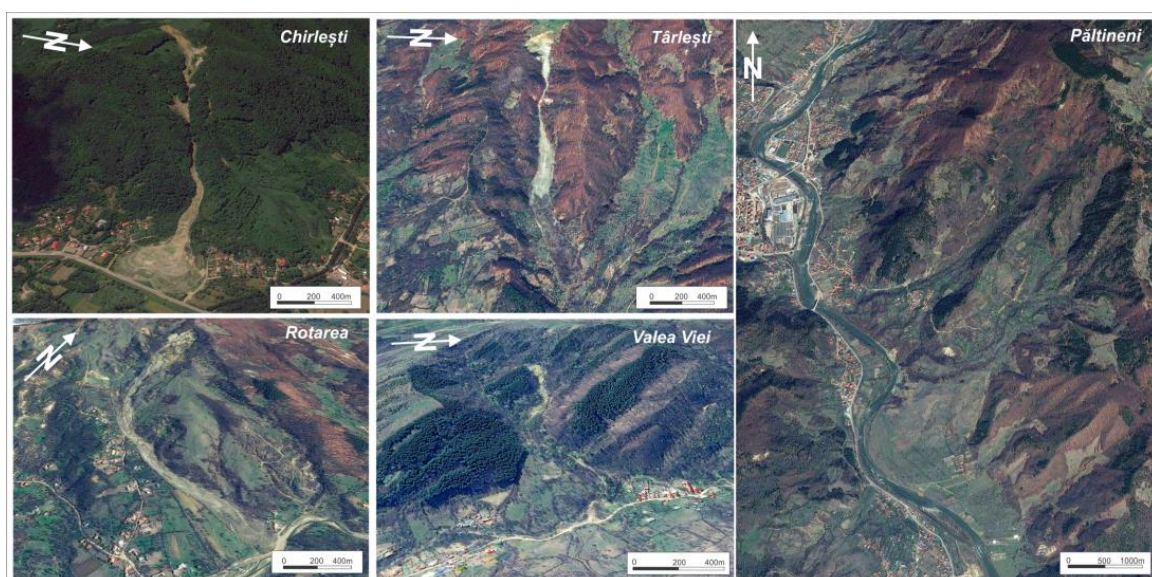


Figure 3. The magnitude of Păltineni landslide in comparison with present-day representative earth/debris flows from the study area. Image source: Google Earth image archive.

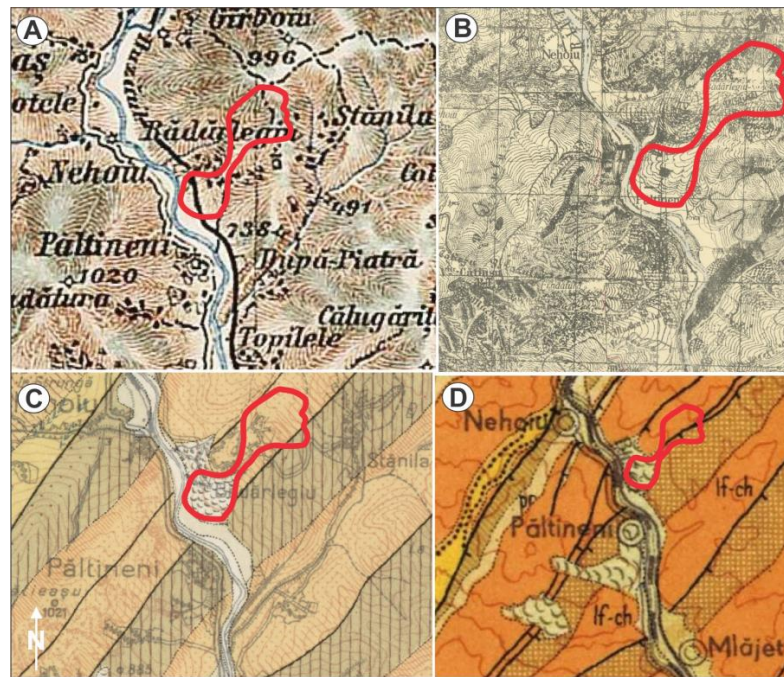


Figure 4. The Pältineni landslide (with red line, the approximated contour) represented on various thematic maps: 1869, 1:200,000 military topographic maps (A); 1924 Lambert–Cholesky 1:20,000 military maps (B); 1:100,000 geological (archive) map of the National Geological Committee, Cheia sheet (C); 1:200,000 geological map [42] (D). Data source (A,B): <https://geo-spatial.org/vechi/download/> (accessed on 7 August 2023).

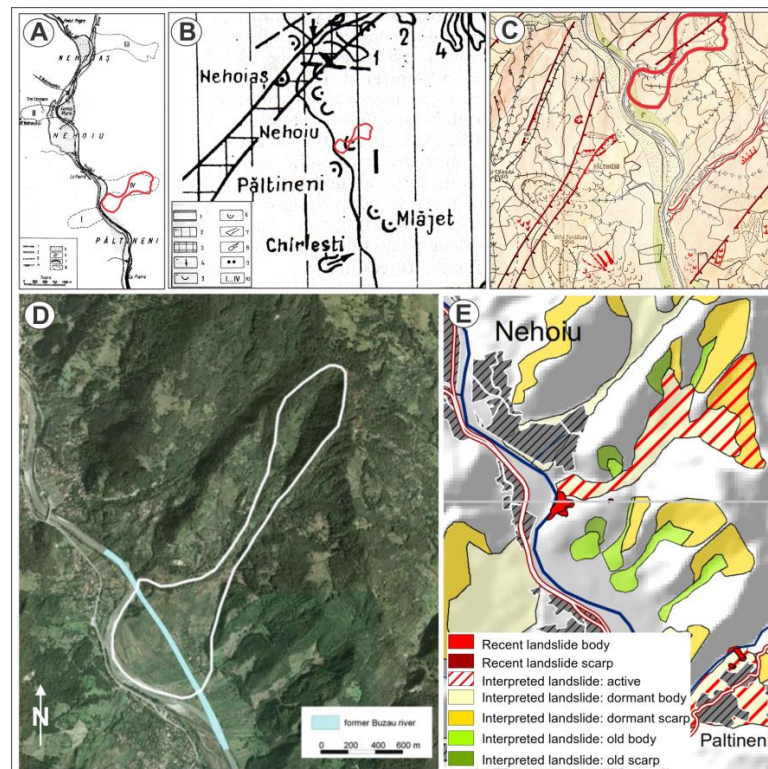


Figure 5. The Pältineni landslide (with red line, the approximated contour) represented on various geomorphologic maps and sketches: [43] (A); [44] (B); 1:25,000 geomorphological map, Pältineni Sheet [45] (C); [39], (D); [40] (E).

3. Materials and Methods

In order to gather consistent information about the landslide's morphology, two directions were employed: field geomorphic mapping and airborne laser scanning. For a more accurate evaluation of the river obliteration process, as well as of the coverage of alluvial deposits by landslides, geophysical surveys were performed.

Geomorphological (including field and lab) mapping was performed during the season without vegetation (November–March) for better visibility and in order to understand the morphologic complexity of the entire slope sector. The main support document was the hillshade model of the LiDAR-derived Digital Terrain Model (DTM). The lab mapping was supported by a (less accurate, but suggestive enough) regional anaglyph 3D visualization (using 1:5000 aerial images from 2008 and the LiDAR-derived DTM) created in the “stereopair from DTM” module of ILWIS Version 3.4 software. The anaglyph interpretation, translated into field mapping points and areas of interest, focused on outlining relative morphometry (planar and vertical convex and concave surfaces, steep/less steep slope segments, slope inclination breaks), terrain position and configuration of the landslide elements (scarps, crown, toe, accumulation/depletion sectors) and associated processes (estimated as active and dormant; sheet wash and gully erosion, local slides/falls, water accumulations, e.g., ponds, vegetation anomalies). The landslide activity (old, recent, presently active) was interpreted based on the expert judgment evaluation of relative morphology of scarps, depletion zones and runout and accumulation sectors. Presently active sectors were considered those showing recent (last 5 years) movements/reactivations; the difference between “old” and “recent” relies on their comparison, without assuming a precise age due to the lack (until this paper, but an issue in progress) of absolute age determination.

The UAV LiDAR study employed a TRINITY F90+ UAV fixed-wing drone equipped with a Qube240 LiDAR sensor (Measur, Calgary, AB, Canada) which was used to perform data processing, resulting in valuable and informative geomorphological point cloud representations. In areas characterized by high relief amplitude, this specific drone's capability to maintain consistent data quality is compromised due to the time and space required for altitude adjustment; this limitation impacts the uniformity of point cloud heights and precludes advanced terrain-following capabilities (see Table 1 for a comparison between a multi-rotor drone and the fixed-wing drone used). The flights' details are provided in Table 2.

Due to the nature of the study area's terrain and the operational capabilities of the UAV, there was an instance where the drone encountered flight obstacles due to specific landscape conditions. During our field expedition, we encountered an area characterized by dense vegetation and significant elevation variations, both of which presented challenges for the drone's capability to maintain a stable flight altitude. The dense vegetation obstructed the penetration of laser pulses, and the uneven terrain made it challenging to maintain a consistent height above the ground. As a result of these challenges, our initial attempt to carry out a successful flight above the wider area was unsuccessful. In response, and with the goal of achieving comprehensive data collection, we chose to partition the entire study area into five smaller, more manageable sections (see Table 1). This decision factored in the UAV's enhanced capacity to navigate terrains with significant changes in elevation while maintaining a consistent altitude. This approach was undertaken to overcome the obstacles posed by the intricate landscape and vegetation, aiming to address the challenges presented by the demanding terrain and vegetation across most of the area.

The methodology encompassed the following steps:

1. *Data Acquisition:* The process involved laser emission and reflection, time-of-flight measurement and recording of position and orientation data. To ensure accuracy, GPS and IMU components were integrated to provide precise location information and capture the sensor's motion and orientation during the survey. The drone followed the terrain at a height of 80–120 m with an average point density of 80 points/m², all within an accuracy threshold of less than 5 cm.

2. *Data Pre-processing*: Systematic errors or biases in the sensor's measurements were addressed through calibration. Noise points and outliers were filtered out to enhance data quality. The incorporation of IMU and GPS data, augmented with RTK corrections, facilitated precise georeferencing, thereby elevating the overall data reliability.
3. *Point Cloud Generation*: The point cloud generation process accounted for multiple returns from a single laser pulse, which occurred due to reflections from different surfaces or objects. Each return was recorded separately in the point cloud, providing multiple elevation measurements for each location. This step resulted in different categories, including ground points, vegetation points, buildings and other objects, which was particularly beneficial in vegetated areas.
4. *Point Cloud Classification*: Point cloud classification was carried out to distinguish ground points from aboveground features such as vegetation, buildings and other objects. The classification was performed using the CSF [46] plugin in Cloud Compare (Table 3), which utilized a 3D computer graphics algorithm based on cloth simulation. This allowed the extraction of ground points from the LiDAR point cloud, effectively separating it into ground and aboveground points.
5. *Digital Terrain Model Generation*: The DTM encapsulated the bare earth surface, achieved by filtering out the non-ground points from the previously classified point cloud (Figure 6). This filtration rendered a refined depiction of the natural terrain topography, omitting aboveground attributes. The ultimate gridded representations of the DTM were derived employing a grid-based interpolation technique, specifically Delaunay triangulation, with a designated cell size of 0.25 m.
6. *Data Export*: The processed data, the point cloud and the DTM were exported as raster files, facilitating further analysis and utilization in geomorphological evaluation and mapping.

Table 1. The capabilities of the fixed-winged drone used in the study in comparison with a multi-rotor one.

Aspect	Multi-Rotor Drone	Fixed-Wing Drone (Trinity f90+)
Flight time	Shorter flight times due to energy demands	Longer flight times due to aerodynamic design
Maneuverability	Highly maneuverable, can hover and change directions quickly	Less maneuverable, requires space for takeoff and landing
Coverage	Suitable for smaller, more detailed areas	Suitable for larger area coverage
Terrain adaptability	Better suited for following terrain in areas with high relief amplitude due to hover and slow-flight capabilities	Challenged by areas with high relief amplitude as it requires space and time for the drone to adjust altitude, especially at a speed of about 18 m/s

Table 2. Information concerning UAV LiDAR flights.

Aspect	Mission 1	Mission 2	Mission 3	Mission 4	Mission 5
UAV model			Trinity f90+		
Sensor model			Qube 240		
Flight height (m)	105	110	85	85	100
Number of points in cloud	231,785,663	224,859,106	148,990,858	304,908,982	224,603,685
Point cloud resolution (points/m ²)	90	85	110	110	95
Surface (ha)	268	272	257	237	260
DEM resolution	0.25	0.25	0.25	0.25	0.25

Table 3. CSF plugin parameters in CloudCompare.

Parameter Name	Description	Value	Options/Units
General Parameters			
Scenes	Set the scene type for the point clouds to determine the terrain's rigidity	Steep slope	Steep slope, relief, flat
Slope Processing	This option fine-tunes the cloth fit to better match ground measurements	On	On/Off
Advanced Parameters			
Cloth Resolution	Refers to the grid size of the cloth used to cover the terrain	0.6	Units of point clouds
Max Iterations	Refers to the maximum iteration times for terrain simulation	600	
Classification threshold	A threshold to classify the point clouds into ground and non-ground parts based on the distances between points and the simulated terrain	0.5	Units of point clouds

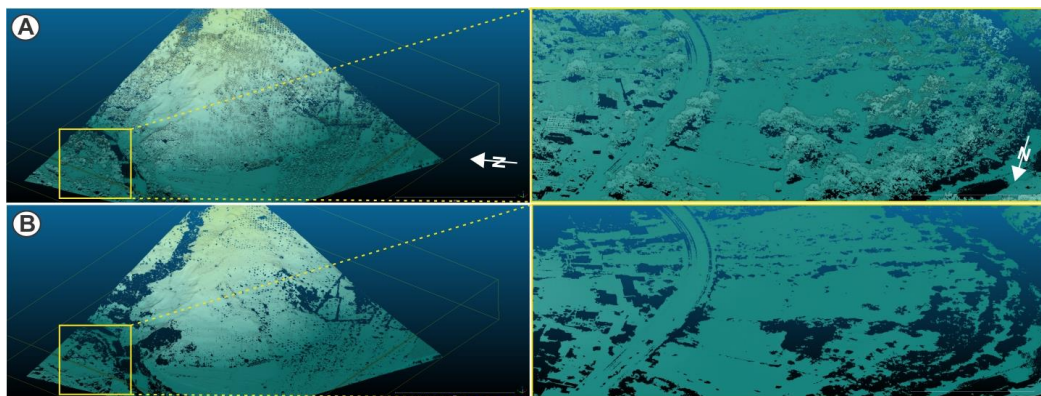


Figure 6. Filtration of ground/non-ground points in case of vegetation and constructions in the accumulation fan area: the largest sample of the point cloud (**left**), without classification and a detailed subsample of a smaller area from the same cloud point (**right**), are shown in subfigure (**A**), while subfigure (**B**) exclusively displays the ground points to its left, and the same detailed subsample with ground points only to its right.

Geophysical investigations involved electrical resistivity tomography (ERT), a technique used for imaging subsurface structures and variations in electrical resistivity, with the purpose to identify potential slip surfaces, determine subsurface water content and map geological structures (like layering, subsurface geology, bedrock depth, etc.) [47,48]. Aiming to outline a potential limit between landslide and river terrace deposits, ERT was employed based on the principle that the two different materials have varying electrical resistivity [49]. By injecting electrical currents into the ground and measuring the resulting potential differences, ERT was used to create 2D images of subsurface resistivity variations. At the Pältineni site, the ERT technique was applied along five profiles (P1–P5) distributed

over the lowermost part of the landslide, at the contact of its accumulation sector with the Buzău River terraces and present floodplain formations. P1 and P2, respectively, and P4 and P5 overlap by two-thirds of their lengths. The ERT data were collected using a GEOTOM MK8E1000 high-resolution multi-electrode instrument (Reunita Research Infrastructure, Penang, Malaysia) from GEOLOG with 75 electrodes. The electrodes were spaced at intervals of 4 m along the profile line, and the maximum profile length was 295 m. The location of each electrode was recorded using a differential GPS (Topcon Hiper V, Topcon, Tokyo, Japan). By combining the data from multiple quadrupole measurements taken in the Wenner configuration, a comprehensive two-dimensional resistivity model of the subsurface was obtained. This model allowed us to visualize the distribution of electrical resistivity in the ground and identify areas with different water contents and material properties. The data inversion, which estimates the true resistivity distribution of the subsurface from the measured apparent resistivity data, was performed using the 2D inversion algorithm of [50] implemented using the RES2DINV (v3.57) software.

4. Results and Discussion

4.1. UAV LiDAR DTM

After collecting data from each individual subsection (see Table 1), the obtained information was merged in order to create a gridded digital terrain model (DTM) with a cell size of 0.25 m. This method allowed us to effectively manage the complex morphology of the wider study area while accommodating the UAV's flight capabilities and limitations. In this way, a complete image of the entire slope–channel system was produced.

4.2. Geomorphologic Interpretation

Based on the correlation and complementarity of field mapping and UAV laser scanning, we were able to understand the entire slope sector morphology, as well as the several sequences that led to the present-day complexity of this deep-seated landslide. Using a hillshade model of the UAV-derived DTM, backed up by a slope map (combined or singularly evaluated during a visual interpretation), several key geomorphic elements, some of them otherwise almost impossible to be recognized during the field mapping due to the dense vegetation cover, were outlined. These elements characterize both forested as well as non-forested sectors of the landslide, and feature both the general depletion and the accumulation sectors. Meanwhile, they allowed us to analyze the landslide persistence, starting with the presumption that during the occurrence moment, a landslide shows a characteristic morphology which can and will be modified through its evolution by natural or human-conditioned processes. The interpreted results were subsequently confirmed by field observations.

In Figure 7, the following elements can be seen: different morphodynamic sectors (active and dormant accumulation and depletion) showing several stages of activity; different magnitude scarps (more recent and older ones, as well as presently active morphologic lineaments) outlining several cases of first-time failures and subsequent reactivations as well; landslide deposit reactivations (either river-induced, resulting from the slope undercut due to lateral erosion of Buzău River, or non-river-induced); erosional forms (gully erosion forms, with different depths, results of different periods of incision of the landslide deposit after its accumulation and thus a relatively older/younger age, steep bare slope, presently modeled by sheet wash associated with low magnitude rock falls); and fluvial forms (Buzău River terraces or ponds across the landslide accumulation deposit). The more-or-less distinct morphological features (like main or secondary, old, recent or active scarps, lateral flanks and contact with the non-landslide-affected deposits of its vicinity, internal morphology, or toe longitudinal and transversal profiles) visible during the analysis of the shaded relief and slope maps were useful in outlining several age stages. Field interpretation confirmed the boundaries of different depletion and accumulation elements (escarpments with various heights, pressure ridges, depressions with stagnating water,

gullies, sheet erosion, etc.), from very visible to less distinct and faint morphological signs on the topographic surface.

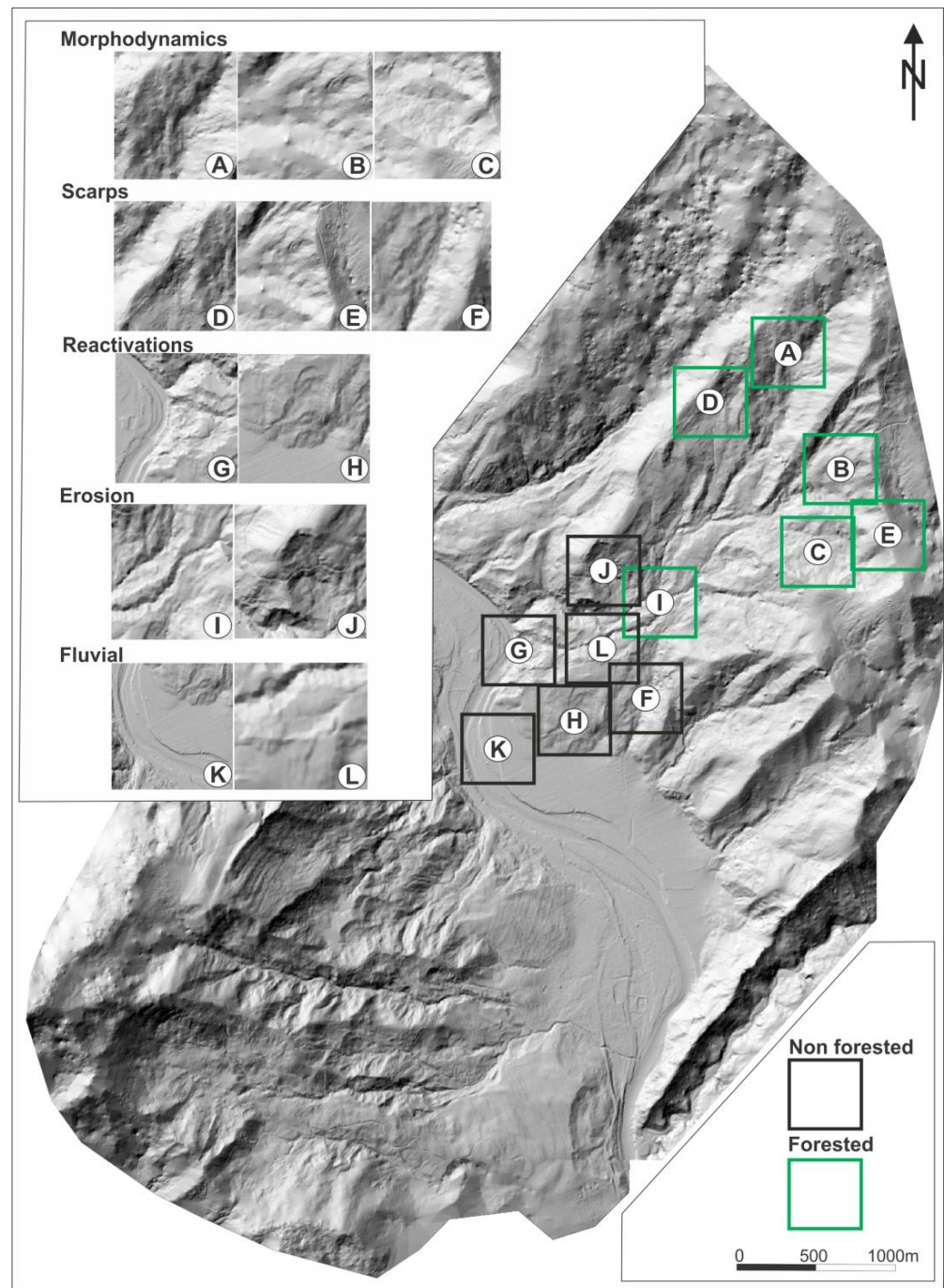


Figure 7. UAV LiDAR hillshade DTM of the study area. Forested/non-forested perimeters characterizing the general depletion/accumulation sectors and containing key geomorphic elements: different morphodynamic sectors (active—A; dormant—B; accumulation/depletion—C); different magnitude scarps (recent—D; old—E; active—F); landslide deposit reactivations (river-induced—G; non-river-induced—H); erosional forms (gully—I, steep bare slope, with sheet wash associated with rock falls—J); and fluvial forms (river terraces—K; pond—L).

All these elements allowed us to obtain a geomorphological map, based on which the relative ages of different sectors, one with respect to the other (dormant—ancient and recent—and presently active), could be observed (Figure 8). Taking into account

the morphology, morphometry and overall magnitude of the geomorphic processes and resulting forms, three stages of activity (and, accordingly, connectivity) were noticed:

- **The dormant ancient landslide:** With a buffered geomorphologic impact and a null superior impact surface, the first landslide (which we assume to be a first-time failure, taking into account the morphological characteristics of such processes in the study area, as described by Ielenicz [38]) remained suspended on the slope, without reaching the Buzău Valley. Occurring in the upper catchment of a small, second-order tributary, it developed as an alternation of translational and rotational (mainly retrogressively, towards the main scarp, as the crown was reducing in size) shallow-to-medium-seated landslide (earth, debris and even small rock slides), outlining a 20 ha depletion area, bordered by a 5–10 m scarp, close to the watershed and presently discontinuous, flattened during a longer evolution, and thus difficult to be sharply recognized. All these considerations suggested an older age, expressed in relative terms by comparing it to the following one. The accumulation of the heterogeneous landslide material is presently noticeable through a hummocky landscape marked by scattered, mostly buried large sandstone blocks. The accumulation deposit (2–5 m thick), presently largely flattened and without obvious rugosity (or cracks and fissures), at its maximum extent, advanced progressively for a short distance along the second-order stream and it stopped, remaining suspended. There is no clear evidence as to how long it advanced, but taking into account local morphological features (especially related to the local lateral extension and longitudinal profile), we assumed that the travel distance was short, of the order of some tens of meters.
- **The dormant recent landslide:** This occurred during the time period following the first (old) landslide, but without clear definition of its time span. It progressively affected the entire longitudinal slope profile, along the second-order stream (left tributary of the Buzău River). Its younger age (in comparison with the first one) was estimated by comparing the aspect of the scarps (flattened and faded in the first case, very much visible and even largely active, determined through retrogressive development, in the second case), the overall morphology of the depletion zones (with better outlined erosional and gravitational processes in the case of the recent one, deeper incised and active gullies, especially in the middle sector, where the two accumulation deposits are overlapping, and fresh rock fall accumulations) and the better-pronounced micromorphology and increased overall rugosity (including clear cracks and fissures) of the landslide deposit. Both depletion and accumulation sectors are marked by active processes (erosional—sheet wash, gully erosion—as well as gravitational—rotational and translational shallow debris and earth slides). The elongated scarps (reaching even 10–20 m in height), situated in the immediate vicinity of the watershed, present numerous sectors (2–10 m high) marked by recent activity (debris and rock accumulations at their foot), despite being largely forested. The large extent of the depletion area (60 ha), the 600 m long and the 60–160 m relatively narrow runout channel and the very large terminal accumulation fan (35 ha) indicate a (most likely) sudden occurrence: the 2–5 m debris deposit (in the median part) and an area up to more than 60–70 m thick (in the final, accumulation fan part) moved progressively along half of the entire slope's longitudinal profile, along the second-order stream, ending with an occlusion geomorphologic impact, during which the Buzău River was shifted with some 500 m westwards, as well as an areal impact surface. The lack of older lateral pressure ridges along the present runout channel or in its immediate vicinity and the compact morphology of the accumulation fan strongly suggest a single pulsation (in comparison, several generations of terminal fans, each one deposited according to a certain pulsation, may be easily witnessed to other similar processes in the immediate vicinity, like the Chirleşti earth flow [36]). Meanwhile, this sudden accumulation of landslide deposits on top of alluvial formations were documented through geophysical measurements, as detailed below.

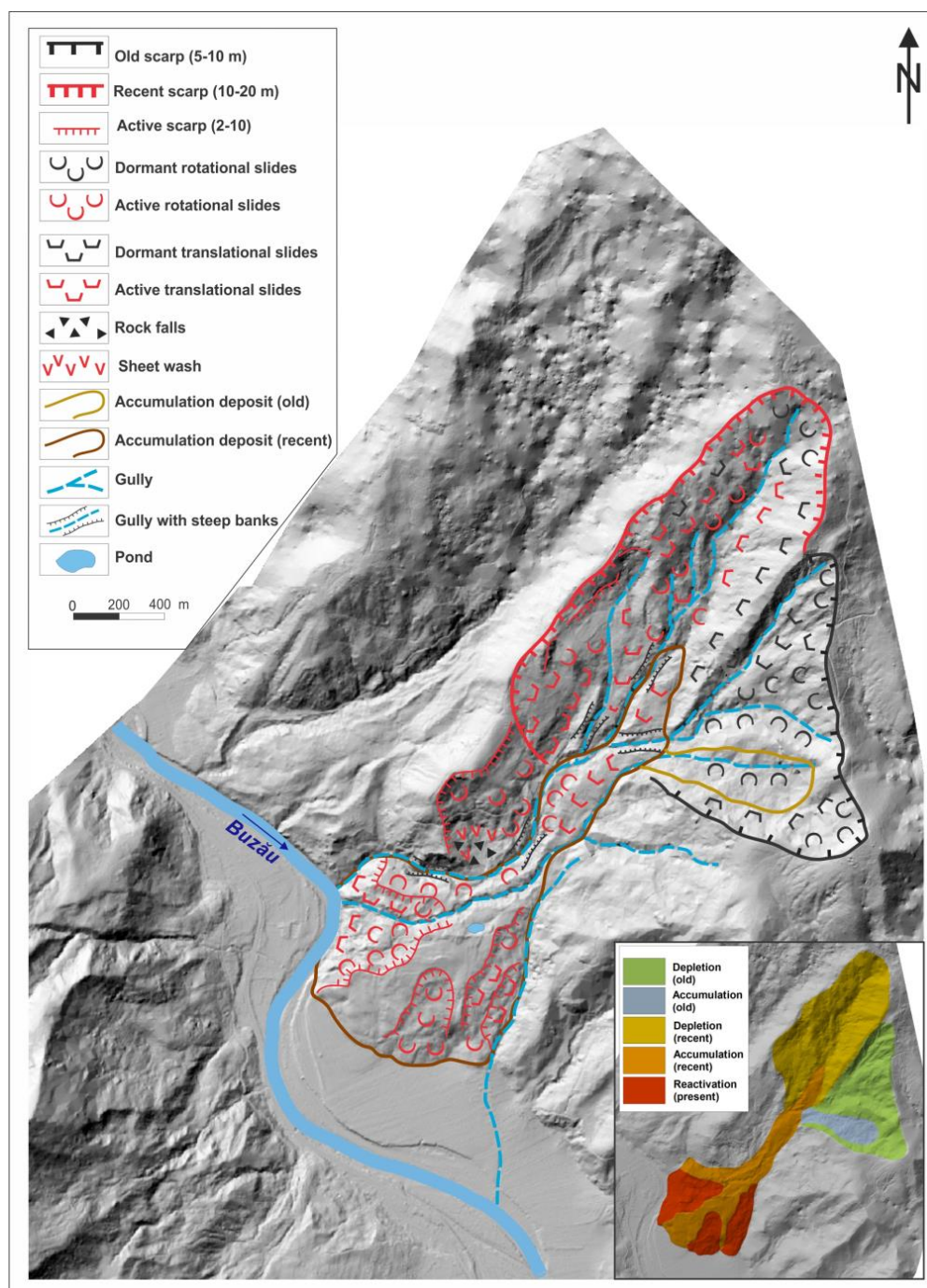


Figure 8. Geomorphological map of the Păltineni landslide. The medallion depicts the relative ages of the different sectors, one with respect to the other (dormant ancient, dormant recent and presently active).

- The presently active sectors:** Corresponding to shallow- and medium-seated reactivations (mainly in the rotational form, but also as translational debris slides) of the landslide toe, these sectors are witnessing the reactivation role of slope gravitational and fluvial processes (see Figure 9). The reactivations are conditioned either by the lateral erosion of the Buzău River (the NW one), as a response of the river's return to its normal hydraulic flow parameters, or by the adaptation of the toe's steep profile (inclinations of up to 15–25°) to the local base level (S and SE ones; the latter is equally conditioned by erosion exerted by the gully which forms the limit between the land-

slide deposit and the in situ rock). A similar process of slope undercut due to river lateral erosion was witnessed immediately north, where the toe of an even older, but similar (at least in morphology) debris flow was completely cut by the Buzău River, which straightened its course once the landslide accumulation deposit was removed. With a more reduced magnitude (1–2 ha each), these presently active sectors show a riparian geomorphologic impact and a linear impact surface (the NW one), as well as a buffered geomorphologic impact (S and SE ones, showing no clear physical contact between the landslide toe and the river) with a null impact surface (the landslide, with both its sectors, depletion and accumulation, is geomorphically decoupled by the river channel).

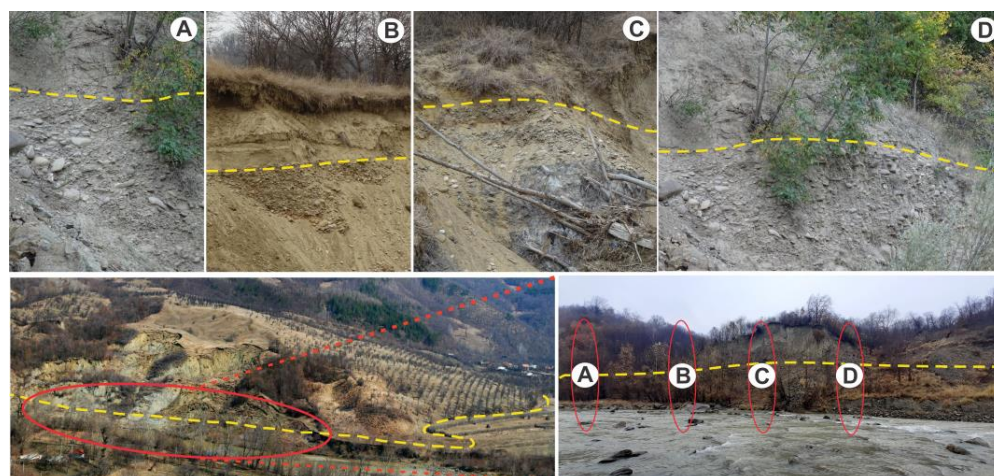


Figure 9. The overlay of landslide deposits (**upper parts**) on top of terrace deposits (**lower parts**) is reflected by the specific morphology and granulometry, as seen along the lineament of river undercut in several representative places (A–D).

The accumulation fan and the toe sector are considered key areas for demonstrating a high-magnitude pulsation (thus supporting the presumed sudden character of displacement and accumulation), leading to the large accumulation of the landslide deposit on top of the alluvial formations. In order to back up the geomorphic assumptions, initially derived only from the analysis of outcrops resulting from the lateral river erosion, a sub-surface characterization of the terminal Păltineni landslide sector using an ERT (another in situ technique) survey was performed. Figure 10 reveals the results of the ERT survey, presenting resistivity values ranging from 5 to 550 Ωm . Most resistivities are relatively low (<80 Ωm), indicating highly conductive materials. However, a relatively resistive layer (>80 Ωm) is observable in the downslope part of all the profiles. The resistive body is more extended in the lower part of the P1 and P4; it partially crosses the present floodplain area of Buzău, but it can also be noticed in the lower parts of P2, P3 and P5. The resistive body occurs on the surface in the floodplain area (P1 and P4), and at some depths in the other profiles. In both P1 and P4, the thickening of the low-resistive layer upslope is obvious. Even if it is not as pronounced, the same pattern is present in P2, P3 and P5. The overlapping profiles (P1 and P2, respectively, and P4 and P5) show good coherence in the measured resistivity values. The analysis of the ERT profiles suggests two distinctive layers at the ERT survey site: a pre-existing, more resistive body on a flat floodplain and low-resistive sediment upslope.

The low-resistive sediments are identified as landslide deposits that have settled on top of the pre-existing alluvial sediments, which are more resistive. This layering is observed explicitly at the front edge of the landslide (e.g., P1 and P4). The thickness of the landslide deposits increases from 15–20 m (in P1 and P4 at the landslide foot) to more than 60–70 m in P2 and P5. Because the maximum penetration depth in the central part was 60–70 m, the slip surface was not reached in the upslope profiles (P2 and P5) or was not detected. Within

the landslide body, we could not distinguish any other distinctive layer of a potential different (previous) age, characterized by particular physical or mechanical properties different from the present ones. The low resistivities related to the landslide body suggest that the content of clay and/or marl is probably considerable in the lower part of the landslide body. In contrast, the alluvial deposit mainly consists of sand and gravel. Due to the difficult accessibility, resistivity measurements were not conducted in the upper part of the Pältineni landslide to check if there was an upslope–downslope variation in the degree of rock grain size distribution. However, making a comparison with the Balta landslide, situated 6 km to the NE, with rather similar morphological and litho-structural conditions, we can assume consistent similarities. As described in [51], similar ERT measurements revealed, in that case, higher resistivity values (around 350 Ωm) close to the detachment scarp and lower resistivity values downslope, where the content of the moisture in the landslide body also increased considerably. However, Balta is a rockslide characterized by a higher concentration of sandstone blocks compared to Pältineni, and this might explain the differences in their resistivities.

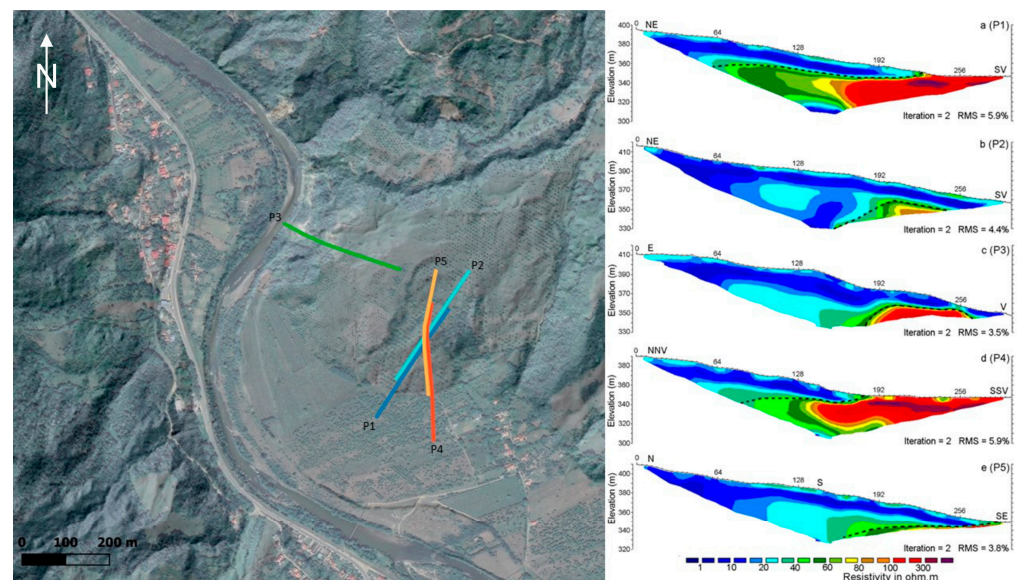


Figure 10. Location of ERT survey lines (profiles 1 to 5) and the inverted ERT profiles of the Pältineni landslide. Their positioning is related to the attempt to outline the overlap of landslide deposits on top of alluvial ones. The dashed line represents the contact between the landslide and the alluvial deposits. Image background: land cover (Map data ©2015 Google) overlay with shaded relief.

Following all the abovementioned considerations, a major issue of interest is represented by the potential triggering factor that might have contributed to such an intriguing landslide. In the study area, shallow landslides usually respond to short-term (24–72 h) precipitation distribution, occurring mainly during the early spring–early summer period, as a result of rain showers which may overlap snowmelt (especially in the regions above 800–900 m a.s.l.). Meanwhile, the same weather conditions are responsible for earth flow pulsations, and several triggering thresholds have been derived [26]: above 35 mm/24 h, 50 mm in 48 h, above 120 mm in 72 h or above 200 mm/month (representing twice the monthly average). In terms of frequency, all these values have recurrence intervals of less than 5 years. In the meantime, deep-seated landslides represent more complex phenomena in terms of triggering factors, and the literature often outlines more than just one [26–28]. The occurrence interval covers almost the entire year (with reduced probabilities during the winter), and peak probabilities characterize the end of spring–beginning of summer, when the groundwater accumulation reaches the maximum due to snowmelt and precipitation. Due to their morphogenetic complexity and due to the lack of a representative number of well-studied case studies, only some estimations (emphasizing the impor-

tance of 1–3 months of antecedent wet intervals) of precipitation triggering thresholds are available: 50 mm (1–3 days), with a return period of 100 y; 60–140 mm (10–30 days), with a return period of 10–35 y; and above 250 mm (1–60 days), with a return period of 30 y.

In this framework, the morphologic evolution of the Pältineni landslide, as proven by the high-accuracy map that resulted from the LiDAR scan, is considered very important since it shows that, despite several stages of activity (dormant ancient, recent, active), there is one which leaves the most important topographic imprint; even so, a comparison with similar present-day similar landslides highlights an obvious difference in magnitude, expressed both in affected areas as well as in displaced volume. The records span over the last century and show similar volumes displaced by slow, deep-seated complex landslides (for example, the Groapa Vântului complex landslide, described by Micu and Bălțeanu [52], or by large rock slides, like the abovementioned Balta landslide), but never by flow-like processes. In the study area, flow-like processes usually respond, in the form of major pulsations, to excessive precipitation, concentrated in short time intervals, especially during the warm and humid period extending from May to July [22]. From this point of view, if we consider only precipitation as the main triggering factor, a relict character (climatic conditions completely different from the present-day ones) of the landslide is assumed. However, the geomorphic mapping revealed clearly outlined geomorphic processes and resulting forms, out of which numerous show obvious signs of recent and present activity. In this case, another additional trigger, typical for the broad study area (the Vrancea seismic region) should be considered: earthquakes. If we consider a climactic trigger for the dormant ancient landslide, we should assume a potential multi-hazard scenario for the recent landslide, such as:

- Independent events or those that change each other's preparing framework (first an earthquake, triggering, in the context of local amplifications, rock falls and shallow landslides in the vicinity of the ridge, resulting in the accumulation of a potentially unstable deposit, with low cohesion and increased permeability, prone to a subsequent rainfall-induced displacement).
- Coupled events (high-magnitude seismic shaking and co-seismic landslide). Clear signs of earthquake-induced landslides are associated with high-magnitude earthquakes, exceeding $M_w > 7$, in both dry and humid conditions [35]. Moreover, knowing that for large, deep-seated landslide initiation, extended periods (7–180 days) with precipitation are needed and the return period of heavy precipitation (FR10) and very heavy precipitation (FR25) range from 30 to 100 years [26,27], one should assume that at least 1–3 times per century, the Vrancea seismic region faces a propitious multi-hazard (large earthquakes and heavy precipitation) scenario, resulting in major geomorphic impacts of deep-seated landslides on river networks.

Following the UAV LiDAR DEM-supported geomorphological mapping, several characteristics of structural connectivity were revealed. Without the high-accuracy DEM, geomorphological mapping would have been largely obstructed by the dense vegetation, and the possibility to clearly outline the three stages of activity would have been very much reduced. The Pältineni landslide offers a representative case in terms of understanding the structural connectivity, and its main characteristics (as summarized in Table 4) may be replicated when, following a bottom-up approach, regional single- and multi-hazard assessments are conducted starting from representative case studies. At the interface of such slope–channel domain interactions, several typical stages (each corresponding to a potential single-to-multi-hazard evaluation approach) can be seen: rather frequent (every 1–5 years), under the effect of single triggers (or multiple triggers, with low magnitudes, changing each one's preparing framework), shallow- and medium-seated landslides may occur (1), remaining suspended on the slopes, completely decoupled (or, at the maximum, indirectly and intermittently coupled in case of overland flow) and making no contact with the channels. Under the effect of single or coupled triggers of a higher magnitude (long-lasting or heavy precipitation, high-magnitude earthquakes), the slope and channel systems may become directly coupled (2) through an occlusion/blockage/obliteration/geomorphic

impact resulting from the progressive advancement of landslide deposits within a single- or multi-hazard framework. In comparison with the size and displaced volumes of similar present-day landslides, the Pältineni landslide exceeds the normal, single-trigger frameworks of the last decades, turning it into a highly likely candidate for a couple-triggered one. Such a multi-hazard framework can be witnessed in the Vrancea seismic region 1–3 times per century, and modern technological developments will allow for the quantification of similar future high-impact events beyond the descriptive approaches (politically and economically) conditioned by the previous lack of measurements. Once the hillslope–channel coupling is set, it remains active for decades (through local reactivations, episodically coupled through shallow landslides, gully erosion and sheet wash). According to the topography, two sectors remain primarily subjected to present-day activity (3): the toe (in case of occlusion or riparian geomorphic impacts) and the scarp/crown (which can evolve through retrogressive failure, conditioning indirect, diffuse and episodic coupling).

Table 4. Main characteristics of structural connectivity resulting from the LiDAR DEM-supported morphological evaluation of the Pältineni landslide.

N°	Coupling	Geomorphic Impact	Impact Surface	Trigger	Single/Multi-Hazard	Recurrence
1	Decoupled/ indirectly coupled	Buffered	Nil	<ul style="list-style-type: none"> Single: Slightly above-average precipitation (both short-term and monthly averages); $M_w > 4.5$ earthquake (with site effects) 	<ul style="list-style-type: none"> Single-hazard Multi-hazard (changing each one's preparing framework) 	1–5 years
2	Directly coupled	Occlusion/ blockage/ obliteration	Areal/ linear	<ul style="list-style-type: none"> Below Pältineni's magnitude: <p>Single (1–3 months antecedent wet intervals or 0–72 h heavy precipitation exceeding 1–2 times the monthly averages); $M_w > 7$ earthquake (in dry/humid conditions)</p> <ul style="list-style-type: none"> Pältineni's magnitude: <p>Multiple (combination of above)</p>	<ul style="list-style-type: none"> Below Pältineni's magnitude: <p>Single hazard</p> <ul style="list-style-type: none"> Pältineni's magnitude: Multi-hazard (coupled events) 	1–3 per century
3	Directly coupled	Riparian, suspended	Linear/ punctual	<ul style="list-style-type: none"> Single: On-site (slightly above-average values) or distant (floods) precipitation; <p>$M_w > 4.5$ earthquake (with site effects)</p>	<ul style="list-style-type: none"> Single hazard Multi-hazard (changing each one's preparing framework) 	1–5 years

5. Conclusions and Perspectives

Understanding the connectivity patterns in case of complex, deep-seated landslides represents a challenging task. Evaluating the present morphology, the morphodynamics sectors and, overall, the morphogenetic framework of such landslides relies on accurate geomorphic mapping, which may be a challenging task in case of old, dormant landslides densely covered by vegetation. If understanding and quantifying connectivity is difficult even in the case of a single process, shifting from the local to the catchment scale still remains one of the main issues in the attempt to understand, explain and quantify how the process of erosion and sediment transport and transfer interact and result in larger, broader-scale geomorphic processes and landscape patterns.

Generally speaking, the landslide-prone environment of the Curvature Carpathians of Romania (the Vrancea seismic region) offers, in perspective, an optimal framework to evaluate local and regional connectivity, as numerous valleys are presently witnessing the long evolution of the slope–channel interface under climatic and seismic triggers. Figure 11 shows a representative image: in a 6 km long valley sector comprising the Păltineni landslide, the riparian geomorphic impact can be measured along 2.6 km, the buffered impact along 2.4 km and the occlusion along 0.6 km. Moreover, the region is currently missing substantial information regarding deep-seated landslides, which is needed for the proper regional evaluation of hazard and risk. New technological advancements may provide a consistent support in local-to-regional mapping, and this paper aims to point towards the fundamental and applied importance of bottom-up approaches, intending to provide accurate regional evaluations based on representative case studies.

In particular, the case of the Păltineni landslide offers a very good example of structural connectivity. Starting from a process which, despite its large magnitude, was barely mentioned in previous geomorphic evaluations, we outlined a complex phenomenon with major implications in both slope and channel evolution. Beginning with buffered geomorphologic impacts and null-impact surfaces, such a deep-seated landslide can evolve, during several stages of initiation/reactivation, leading to an occlusion (and even obliteration) geomorphologic impact (in this case, the most important local river crossing that Carpathian sector suffered from a 500 m lateral shift of its course, as the result of a sudden blockage with landslide deposits) and large, areal impact surfaces. For understanding the complexity of such deep-seated landslides and the connectivity they can be responsible for, geomorphic mapping is vital, but many times challenging. Relict, old and recent, and dormant and active depletion and accumulation sectors are usually interfering, and dense vegetation cover can make the field mapping difficult. To overcome these challenges, UAV LiDAR-derived DTMs represent reliable data sources for accurate geomorphic mapping, especially in forested areas.

Bringing the case of the Păltineni landslide to a more general, regional setting, it results that the landslide we have evaluated is not just a singular phenomenon, and numerous such examples can be recognized along the main valleys.

From a fundamental perspective, such landslide processes represent key elements in understanding the long-term evolution of slopes and channels in their continuous interaction; meanwhile, from an applied perspective, the same interaction provides vital information regarding multi-hazard assessment through cascading effects. Moreover, the present-day development of tourist activities along the main valleys that cross the Carpathians in this landslide-prone sector are increasing exposure and vulnerability, making local and regional multi-hazard risk studies a necessary approach within the disaster risk reduction plans.

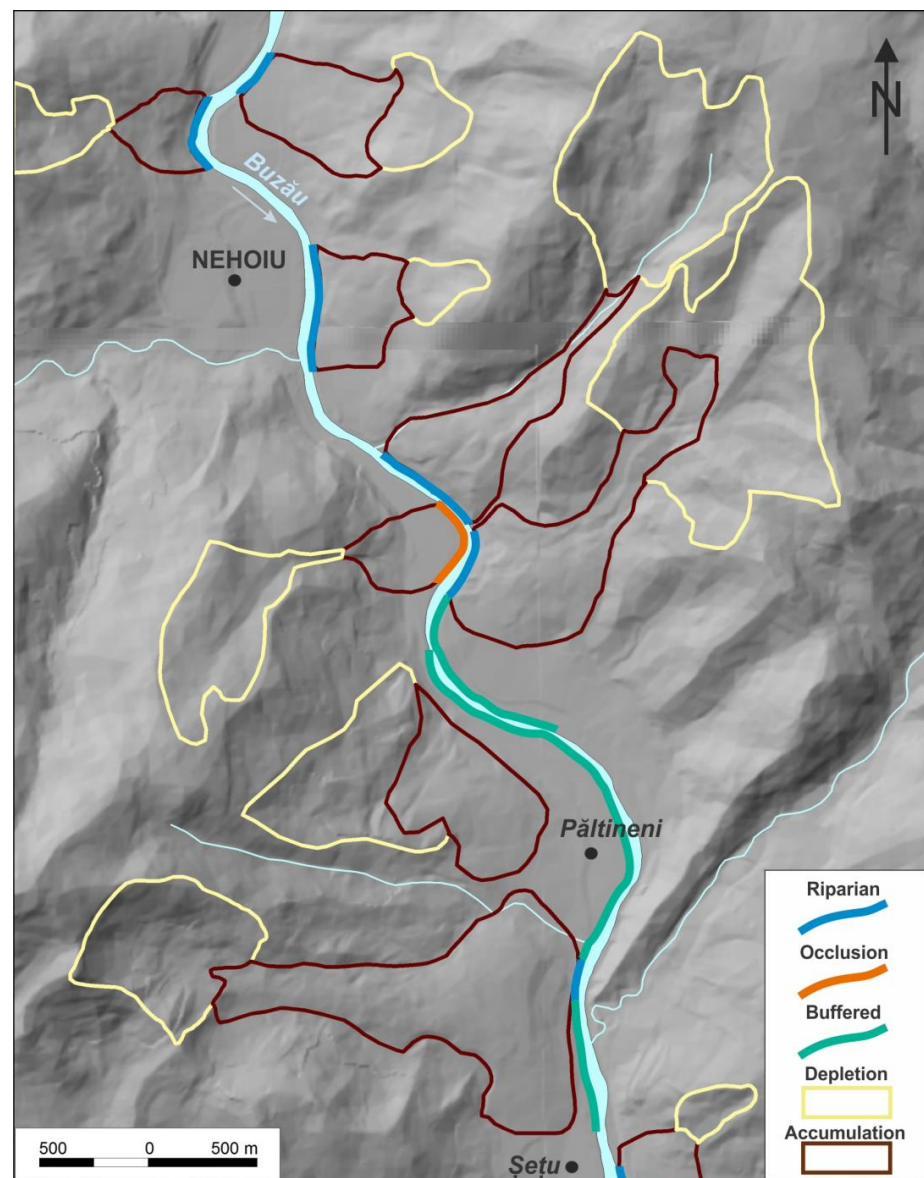


Figure 11. Buzău Valley between the village of Șețu (south of the map) and the town of Nechoiu (north of the map): numerous riparian, occlusion and buffered geomorphologic impact and linear/areal impact surfaces can support the future understanding of catchment-scale connectivity quantification (background: 30m SRTM hillshade).

Author Contributions: Conceptualization, M.M., M.V. and F.M.; methodology, M.M., M.V., F.M., A.O., F.S. and Skyline Drones Team; software, Skyline Drones Team, F.M. and A.O.; validation, Skyline Drones Team, F.M., A.O. and M.M.; field investigation, M.M., M.V. and F.M.; resources, Skyline Drones Team, F.M., M.V. and A.O.; writing—original preparation, M.M., M.V., F.M., A.O., F.S. and Skyline Drones Team. All authors have read and agreed to the published version of the manuscript.

Funding: The research presented here was carried out within the framework of the EEA—Norway Grants 2014–2021, under project code RO-NO-2019-0415/contract no. 30/2020, the research theme “Geographical studies within Patarlăgele Natural Hazards Research Center” of the Institute of Geography of the Romanian Academy (2019–2022) and University of Bucharest, project code C1.2.PFE-CDI.2021-587/contract 41PFE/2021. This research was conducted with the support of the hardware–software infrastructure developed under the project no. 327/390003/06-11-2020, SMIS code: 126867, “Strengthening the research capacity for ecosystem and biodiversity at the University of Bucharest through e-science and technology—Lifewatch Romania”; co-financed under Regional Development Fund (ERDF), Competitiveness Operational Programme”.

Data Availability Statement: The data presented in this study are available on request from the corresponding author. The data are not publicly available due to present ongoing researches and Remote Sensing/GIS database enrichment.

Conflicts of Interest: The authors declare no conflict of interest.

References

- Poljansek, K.; Marin Ferrer, M.; Vernaccini, L.; Marzi, S.; Messina, L. *Review of the Sendai Framework Monitor and Sustainable Development Goals Indicators for Their Inclusion into INFORM Global Risk Index*; Publications Office of the European Union: Luxembourg, 2019; ISBN 978-92-76-03849-8. [\[CrossRef\]](#)
- Shano, L.; Raghuvanshi, T.K.; Meten, M. Landslide susceptibility evaluation and hazard zonation techniques—A review. *Geoenviron Disasters* **2020**, *7*, 18. [\[CrossRef\]](#)
- Davis, W.M. The geographical cycle. *Geogr. J.* **1989**, *14*, 481–504. [\[CrossRef\]](#)
- Penk, W. *Morphological Analysis of Landforms*; McMillan: London, UK, 1953.
- King, L. *The Morphology of the Earth*; Oliver and Boyd: Edinburgh, UK, 1962; p. 726.
- Skempton, A.W. Soil mechanics in relation to geology. *Proc. Yorks. Geol. Soc.* **1953**, *29*, 33–62. [\[CrossRef\]](#)
- Hutchinson, J.N. The Stability of Cliffs Composed of Soft Rocks, with Particular Reference to the Coast of South-East England. Ph.D. Thesis, University of Cambridge, Cambridge, UK, 1965.
- Selby, M.J. Dominant geomorphic events in landform evolution. *Bull. Int. Assoc. Eng. Geol.* **1974**, *9*, 85–89. [\[CrossRef\]](#)
- Carson, M.A.; Kirkby, M.J. *Hillslope Form and Process*; Cambridge University Press: Cambridge, UK, 1972; 475p.
- Crozier, M.J. Landslide Geomorphology: An argument for recognition, with examples from New Zealand. *Geomorphology* **2010**, *120*, 3–15. [\[CrossRef\]](#)
- Korup, O. Earthquake-triggered landslides—Spatial patterns and impacts. In *COGEAR Module 1 Report*; Swiss Federal Research Institutes WSL/SLF: Davos, Switzerland, 2010.
- Chorley, R.J.; Kennedy, B.A. *Physical Geography: A Systems Approach*; Prentice Hall: London, UK, 1971.
- Poeppl, R.E.; Keesstra, S.D.; Maroulis, J. A conceptual connectivity framework for understanding geomorphic change in human impacted fluvial systems. *Geomorphology* **2016**, *277*, 237–250. [\[CrossRef\]](#)
- Wohl, E.; Magilligan, F.; Rathburn, S.L. Introduction to the special issue: Connectivity in Geomorphology. *Geomorphology* **2016**, *277*, 1–5. [\[CrossRef\]](#)
- Wohl, E.; Brierley, G.; Cadol, D.; Coulthard, T.; Covino, T.; Fryirs, K.; Sklar, L. Connectivity as an Emergent Property of Geomorphic Systems. *Earth Surf. Process. Landf.* **2019**, *44*, 4–26. [\[CrossRef\]](#)
- Bracken, L.J.; Turnbull, L.; Wainwright, J.; Bogaart, P. Sediment connectivity: A framework for understanding sediment transfer at multiple scales. *Earth Surf. Process. Landf.* **2015**, *40*, 177–188. [\[CrossRef\]](#)
- Cossart, E.; Fressard, M. Assessment of structural sediment connectivity within catchments: Insights from graph theory. *Earth Surf. Dyn.* **2017**, *5*, 253–268. [\[CrossRef\]](#)
- Heckmann, T.; Schwanghart, W. Geomorphic coupling and sediment connectivity in an alpine catchment—Exploring sediment cascades using graph theory. *Geomorphology* **2013**, *182*, 89–103. [\[CrossRef\]](#)
- Heckmann, T.; Cavalli, M.; Cerdan, O.; Foerster, S.; Javaux, M.; Lode, E.; Brardinoni, F. Indices of sediment connectivity: Opportunities, challenges and limitations. *Earth Sci. Rev.* **2018**, *187*, 77–108. [\[CrossRef\]](#)
- Persichillo, M.G.; Bordoni, M.; Cavalli, M.; Crema, S.; Meisina, C. The role of human activities on sediment connectivity of shallow landslides. *Catena* **2018**, *160*, 261–274. [\[CrossRef\]](#)
- Najafi, S.; Dragovich, D.; Heckmann, T.; Sadeghi, S.H. Sediment connectivity concepts and approaches. *Catena* **2021**, *196*, 104880. [\[CrossRef\]](#)
- Zingaro, M.; Refice, A.; Giachetta, E.; D’Addabbo, A.; Lovergine, F.; De Pasquale, V.; Capolongo, D. Sediment mobility and connectivity in a catchment: A new mapping approach. *Sci. Total Environ.* **2019**, *672*, 763–775. [\[CrossRef\]](#) [\[PubMed\]](#)
- Wainwright, J.; Turnbull, L.; Ibrahim, T.G.; Lexartza-Artza, I.; Thornton, S.F.; Brazier, R.E. Linking environmental regimes, space and time: Interpretations of structural and functional connectivity. *Geomorphology* **2011**, *126*, 387–404. [\[CrossRef\]](#)
- Jain, V.; Tandon, S.K.; Sinha, R. Application of modern geomorphic concepts for understanding the spatio-temporal complexity of the large Ganga river dispersal system. *Curr. Sci.* **2012**, *103–111*, 1300–1319.
- Micu, M.; Micu, D.; Soldati, M. Mass movements in changing mountainous environments. In *Treatise on Geomorphology*; Elsevier: Amsterdam, The Netherlands, 2021; ISBN 9780124095489. [\[CrossRef\]](#)
- Micu, M. Landslide types and spatial pattern in the Subcarpathian area. In *Landform Dynamics and Evolution in Romania*; Radoane, M., Vespremeanu-Stroe, A., Eds.; Springer: Berlin/Heidelberg, Germany, 2017; pp. 305–325.
- Micu, M.; Micu, D. Landslides morphogenetic complexity in the Buzău Carpathians and Subcarpathians. Implication for hazard assessment. *Rom. J. Geogr.* **2022**, *66*, 137–152.
- Micu, M. The systematic of landslide processes in the conditions of Romania’s relief. In *Landform Dynamics and Evolution in Romania*; Radoane, M., Vespremeanu-Stroe, A., Eds.; Springer: Berlin/Heidelberg, Germany, 2017; pp. 249–269.
- Șirbu, F.; Drăguț, L.; Oguchi, T.; Hayakawa, Y.; Micu, M. Scaling land-surface variables for landslide detection. *Prog. Earth Planet. Sci.* **2019**, *6*, 44. [\[CrossRef\]](#)

30. Zumpano, V.; Hussin, H.; Reichenbach, P.; Bălțeanu, D.; Micu, M.; Sterlacchini, S. A landslide susceptibility analysis for Buzău County, Romania. *Rom. J. Geogr.* **2014**, *58*, 9–16.
31. Brock, J.; Schratz, P.; Petschko, H.; Muenchow, J.; Micu, M.; Brenning, A. The performance of landslide susceptibility models critically depends on the quality of digital elevation models. *Geomat. Nat. Hazards Risk* **2020**, *11*, 1075–1092. [[CrossRef](#)]
32. Dornik, A.; Drăguț, L.; Oguchi, T.; Hayakawa, Y.; Micu, M. Influence of sampling design on landslide susceptibility modeling in lithologically heterogeneous areas. *Sci. Rep.* **2022**, *12*, 2106. [[CrossRef](#)] [[PubMed](#)]
33. Havenith, H.; Torgoev, A.; Braun, A.; Schlogel, R.; Micu, M. A new classification of earthquake-induced event sizes based on seismotectonic, topographic, climatic and geologic factors. *Geoenvironmental Disasters* **2016**, *3*, 2–24. [[CrossRef](#)]
34. Kumar, V.; Cauchie, L.; Mreyen, A.S.; Micu, M.; Havenith, H.B. Evaluating landslide response in seismic and rainfall regime: A case study from the SE Carpathians, Romania. *Nat. Hazards Earth Syst. Sci.* **2021**, *12*, 3767–3788. [[CrossRef](#)]
35. Micu, M.; Micu, D.; Havenith, H.B. Earthquake-induced landslide hazard assessment in the Vrancea Seismic Region (Eastern Carpathians, Romania): Constraints and perspectives. *Geomorphology* **2023**, *427*, 108635. [[CrossRef](#)]
36. Jurchescu, M.; Kucsicsa, G.; Micu, M.; Sima, M.; Balteanu, D. Landslide exposure assessment under environmental change in the Romanian Subcarpathians. *Stud. Geomorphol. Carpatho Balc.* **2020**, *53–54*, 59–84.
37. Ielenicz, M. *Munții Ciucaș-Buzău. Studiu Geomorfologic*; Editura Academiei Republicii Socialiste România: Bucharest, Romania, 1984; 148p. (In Romanian)
38. Micu, M.; Bălțeanu, D. The Impact of Deep-Seated Landslides on Reservoirs and Rivers in Vrancea Seismic Region. In *Landslide Science and Practice: Volume 6: Risk Assessment, Management and Mitigation*; Margottini, C., Canuti, P., Sassa, K., Eds.; Springer: Berlin/Heidelberg, Germany, 2013; pp. 117–123. [[CrossRef](#)]
39. Damen, M.; Micu, M.; Zumpano, V.; Van Westen, C.J.; Sijmons, K.; Balteanu, D. Landslide mapping and interpretation: Implications for landslide susceptibility analysis in discontinuous data environment. In Proceedings of the International Conference Analysis and Management of Changing Risks for Natural Hazards, Padua, Italy, 18–19 November 2014; pp. 177–186.
40. Korup, O. Geomorphic imprint of landslides on alpine river systems, southwest New Zealand. *Earth Surf. Process. Landf.* **2005**, *30*, 783–800. [[CrossRef](#)]
41. Bălțeanu, D.; Micu, M. Morphodynamics of the Chirlești mudflow (Buzău Mountains). *Rom. J. Geogr.* **2012**, *56*, 2.
42. Dumitrescu, I.; Săndulescu, M.; Bandrabur, T. *Geological Map of Romania 1:200,000, Sheet 29-Covasna*; Institute of Geology: Bucharest, Romania, 1970.
43. Posea, G. Glissement, méandres et voies de communication dans la Vallée de Buzau. In *Travaux du Symposium International de Géomorphologie Appliquée: Bucarest, Mai 1967*; Institut de Géologie et de Géographie de l'Académie de la République Socialiste de Roumanie: Bucharest, Romania, 1969.
44. Ielenicz, M. Contributii la studiul porniturilor de teren din bazinul superior al Buzaului. *Rev. Pădurilor* **1969**, *2*, 73–76. (In Romanian)
45. Sandu, M. *General Geomorphological Map 1:25,000, Paltineni Sheet*; Institute of Geography: Bucharest, Romania, 1993.
46. Zhang, W.; Qi, J.; Wan, P.; Wang, H.; Xie, D.; Wang, X.; Yan, G. An Easy-to-Use Airborne LiDAR Data Filtering Method Based on Cloth Simulation. *Remote Sens.* **2016**, *8*, 501. [[CrossRef](#)]
47. Reynolds, J.M. *An Introduction to Applied and Environmental Geophysics*; Wiley and Sons: Chichester, UK, 1997.
48. Perronne, A.; Lapenna, V.; Piscitelli, S. Electrical resistivity tomography technique for landslide investigation: A review. *Earth-Sci. Rev.* **2014**, *135*, 65–82. [[CrossRef](#)]
49. Hack, R. Geophysics for slope stability. *Surv. Geophys.* **2000**, *21*, 423–448. [[CrossRef](#)]
50. Loke, M.; Barker, R. Practical techniques for 3D resistivity surveys and data inversions 1. *Geophys. Prospect.* **1996**, *44*, 499–523. [[CrossRef](#)]
51. Mreyen, A.S.; Cauchie, L.; Micu, M.; Onaca, A.; Havenith, H.B. Multiple geophysical investigations to characterize massive slope failure deposits: Application to the Balta rockslide, Carpathians. *Geophys. J. Int.* **2021**, *225*, 1032–1047. [[CrossRef](#)]
52. Micu, M.; Bălțeanu, D. A deep-seated landslide dam in the Siriu Reservoir, Bend Carpathians—Romania. *Landslides* **2013**, *10*, 323–329. [[CrossRef](#)]

Disclaimer/Publisher's Note: The statements, opinions and data contained in all publications are solely those of the individual author(s) and contributor(s) and not of MDPI and/or the editor(s). MDPI and/or the editor(s) disclaim responsibility for any injury to people or property resulting from any ideas, methods, instructions or products referred to in the content.